SAMPLING PATTERN DESIGN ALGORITHM FOR ATOMIC FORCE MICROSCOPY IMAGES

Yufan Luo[1] *and Sean B. Andersson*[1,2]

[1]Division of Systems Engineering and [2]Department of Mechanical Engineering
Boston University, Boston, MA 02215

ABSTRACT

This work focuses on the development of an algorithm to design sampling patterns for acquiring images in atomic force microscopy (AFM). The goal is to reduce data acquisition time of the instrument without significantly compromising image quality by appropriately allocating sampling effort. We assume the frequency structure of the images to be sampled, and in particular the locations of the large frequency coefficients, is partially known. Based on this knowledge, the expected reconstruction error using simplified matching pursuit (SMP) is analyzed and a Monte Carlo-based strategy is proposed to create sampling patterns that minimize the expected error. The proposed method is demonstrated through simulation on two groups of sample surface images from two different materials acquired by AFM.

Index Terms— atomic force microscopy, sampling pattern design

1. INTRODUCTION

Atomic force microscopy (AFM) is a powerful tool for imaging topography or other characteristics of sample surfaces at very high resolution by recording the interaction of a sharp probe with the surface. For a conventional AFM, images are acquired by rastering the tip across the surface, leading to long acquisition times. To increase the imaging rate of the instrument, various approaches have been proposed including improved mechanical design [1, 2], often combined with the use of advanced control algorithms of the image [3–6]. A complementary approach based on undersampling was introduced in [7, 8], in which an increased imaging rate is achieved by reducing the number of pixels to be acquired. The final surface image is created from the measured pixels using image reconstruction techniques from, e.g. compressive sensing (CS) or inpainting.

Compared to inpainting, CS is preferable for reconstructing sparse or compressible images [9]. CS methods seek the true image signal $x \in \mathbb{R}^n$ from the following equation,

$$y = \Phi x = \Phi\Psi\eta \triangleq A\eta \tag{1}$$

where $y \in \mathbb{R}^m$ is the observation vector, Φ is an $m \times n$ matrix defining the measurements, Ψ is an $n \times n$ sparsity basis and η is the sparse representation of x in the domain of Ψ. In general, $m \ll n$. In the AFM application, the probe can only measure a single pixel at a time. As a result, Φ is a sparse matrix with each row having only one nonzero entry. Thus, y is a subset of x. We define $\Phi\Psi$ as the sensing matrix A. It is known that the reconstruction quality for many CS methods depends on the properties of A such as the restricted isometry property (RIP) [10] and mutual coherence [11].

In traditional CS, non-adaptive random sampling, such as selecting to sample each pixel with the same probability, is considered a simple and effective strategy for designing an A with good properties for stable reconstruction. However, random sampling does not offer significantly lower data acquisition time for AFM, since the probe has to visit scattered sampling locations, lifting the probe tip after each measurement and reengaging it to the surface to begin the next pixel. Continuous sampling paths that avoid the need to repeatedly re-engage the tip, such as Lissajous and spiral patterns, are more desirable in practice. In [12], the authors introduced a new sampling pattern for AFM called the μ-path pattern, where small groups of randomly selected pixels are sampled together. Faithful recovery was achieved with Basis Pursuit (BP).

In prior work, the authors used a variant of the Matching Pursuit (MP) algorithm, called Simplified Matching Pursuit (SMP), to reconstruct images sampled with μ-path patterns [13]. SMP is essentially the same as MP except for the reconstruction order of entries in η. Numerical simulations suggest that, for continuous sampling paths and μ-path patterns of large size, SMP performs better than Orthogonal Matching Pursuit (OMP) and CS Matching Pursuit (CoSaMP) in both reconstruction quality and computational time. Therefore, here we focus on μ-path sampling pattern with SMP reconstruction.

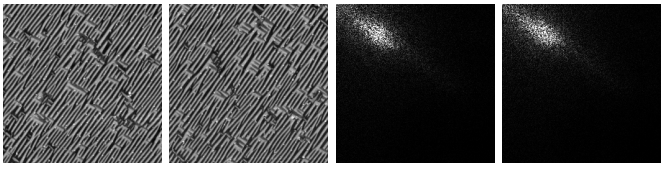

Fig. 1: $18\mu m$ AFM images showing BiFeO3/SrRuO3/DyScO3 and their coresponding DCT domain coefficients.

In AFM, the scanning range of the tip is often limited to between 10-100 μm in the lateral plane. Imaging of larger regions is typically achieved by *tiling*, that is by imaging adjacent, non-overlapping areas and stitching them into a single large image (see Fig. 2). While the spatial details of each of the tiles differs, they often have very similar structure in the frequency domain. Similarly, one often uses AFM to image slowly changing samples where the frequency structure from image to image in the

This work was supported in part by NSF through grants CMMI-1234845, DBI-1352729 and CMMI-1562031.

sequence are quite similar. In both these settings, one can use an initial frame to roughly estimate the locations of the large frequency coefficients for the material (illustrated in Fig. 1). The sensing matrix A can then be designed to focus on these large-coefficient locations, instead of evenly exploring the whole frequency space. Many previous works (e.g. [14–16]) have discussed the problem of sensing matrix design. However, these mainly focus on developing algorithms to minimize mutual coherence and require Φ to be dense. As noted above, such matrices are not feasible for AFM. In [17], the authors suggested a relaxation of a discrete optimization problem for constrained Φ design. However, the analysis is based on the assumption that the locations of nonzero entries in η are known.

In this work, we discuss the criterion for A^TA to minimize the expected reconstruction error with SMP, based on knowledge of the frequency structure of the sample image. A Monte Carlo-based algorithm is proposed to select μ paths to satisfy the criterion. We note that the same analysis can be applied to MP; SMP is used here due to its reduced computational cost.

The following notation will be used. We denote $\eta^{\#}$ as the sparse signal reconstructed with SMP. Denote i' as the index of the entry reconstructed in the i^{th} iteration with SMP and $\mathcal{J} = \{1', 2', ..., j'\}$ as the index set of the entries in η that have been reconstructed by the j^{th} iteration. Denote $\mathcal{T}$ as the index set of nonzero entries in η, $\mathcal{I}$ as the index set of the nonzero entries with known locations and $\mathcal{U}$ as the index set of the nonzero entries with unknown locations. Therefore, $\mathcal{T} = \mathcal{I} \cup \mathcal{U}$. We assume η is a k-sparse image signal. The cardinality of $\mathcal{I}$ is pk and of $\mathcal{U}$ is $(1-p)k$, $(0 \leqslant p \leqslant 1)$. We define

$$\hat{\eta} \triangleq A^T y = A^T A\eta \triangleq S\eta \tag{2}$$

from (1). For a vector η, let η_i be its i^{th} entry. For a matrix S, let $S_{i,j}$ be its i, j^{th} entry.

2. ALGORITHM

In SMP, the unknown image signal η is reconstructed from (2) with one entry recovered in each iteration. Our goal is to design the matrix S (and thus the sampling pattern) based on the information of $\mathcal{I}$ to minimize the expected square error $\min_S \mathrm{E}[\|\eta - \eta^{\#}\|_2^2]$.

Three assumptions are made to simplify the analysis. First, A has a small mutual coherence such that SMP can reconstruct all k nonzero entries in η from the entries with largest magnitude to the smallest. That is, i' is the index of i^{th} largest coefficients in η. This assumption can be verified after S has been designed. Second, all nonzero entries in η are zero mean, independent and identically distributed. Third, for those entries in $\mathcal{U}$, their locations are uniformly distributed in $\mathcal{I}^c$.

Based on the three assumptions, we first consider the case when $\mathcal{U} = \emptyset$, implying we know the locations of all the nonzero entries in η and $\mathcal{T} = \mathcal{I}$. For notational simplicity, we assume without loss of generality that the first k entries in η are nonzero and $\mathcal{T} = \{1, 2, \ldots, k\}$. Let $\mathcal{H} = \{|\eta_1| > |\eta_2| > ... > |\eta_k|, |\eta_2| > |\eta_1| > ... > |\eta_k|, \ldots, |\eta_k| > |\eta_{k-1}| > ... > |\eta_1|\}$ be the magnitude permutation set with $k!$ elements, so each element is an ordered sequence. The estimate of the $(j')^{th}$ entry $\eta^{\#}_{j'}$ with SMP is given by [13],

$$\eta^{\#}_{j'} = \frac{\hat{\eta}_{j'} - \sum_{i=1'}^{(j-1)'} S_{j',i}\eta^{\#}_i}{S_{j',j'}} = \frac{\sum_{i\in\mathcal{T}} S_{j',i}\eta_i - \sum_{i=1'}^{(j-1)'} S_{j',i}\eta^{\#}_i}{S_{j',j'}}. \tag{3}$$

The corresponding estimation error of the $(j')^{th}$ entry is

$$\Delta\eta_{j'} = \eta_{j'} - \eta^{\#}_{j'} = \frac{\sum_{i\in\mathcal{T}\setminus\mathcal{J}} S_{j',i}\eta_i}{S_{j',j'}} + \frac{\sum_{i=1'}^{(j-1)'} S_{j',i}\Delta\eta_i}{S_{j',j'}}. \tag{4}$$

The error is composed of two parts. The first comes from the influence of other entries in η on the current reconstruction, while the second is from the previous estimation errors. When A has small mutual coherence, the first part is much larger than the second part ($|\eta_i| \gg |\Delta\eta_i|$) and therefore the ℓ_2 estimation error of the SMP reconstruction can be approximated as,

$$\|\Delta\eta\|_2^2 = \textstyle\sum_{j\in\mathcal{T}} \Delta\eta_j^2 \approx \sum_{j=1'}^{k'} \left(\sum_{i\in\mathcal{T}\setminus\mathcal{J}} \frac{S_{j,i}}{S_{j,j}}\eta_i \right)^2. \tag{5}$$

In (5), $1', ..., k'$ are random variables defining the ordering of the index sequence in the recovery, given by an element of $\mathcal{H}$. Thus

$$\begin{aligned} \mathrm{E}\left[\|\Delta\eta\|_2^2\right] &\approx \mathrm{E}\left[\sum_{j=1'}^{k'} \left(\sum_{i\in\mathcal{T}\setminus\mathcal{J}} \frac{S_{j,i}}{S_{j,j}}\eta_i \right)^2 \right] \\ &= \sum_{h\in\mathcal{H}} \mathrm{E}\left[\sum_{j=1'}^{k'} \left(\sum_{i\in\mathcal{T}\setminus\mathcal{J}} \frac{S_{j,i}}{S_{j,j}}\eta_i \right)^2 \middle| h \right] \mathrm{P}(h). \end{aligned} \tag{6}$$

Based on the assumption that each entry in $\mathcal{T}$ follows the same distribution, each element in $\mathcal{H}$ occurs with the same probability $\mathrm{P}(h) = \frac{1}{k!}$. Consider when $h = \{|\eta_1| > |\eta_2| > ... > |\eta_k|\}$. Then

$$\begin{aligned} &\mathrm{E}\left[\sum_{j=1'}^{k'} \left(\sum_{i\in\mathcal{T}\setminus\mathcal{J}} \frac{S_{j,i}}{S_{j,j}}\eta_i \right)^2 \middle| |\eta_1| > |\eta_2| > ... > |\eta_k| \right] \\ =&\mathrm{E}\left[\sum_{j=1}^{k} \left(\sum_{i=j+1}^{k} \frac{S_{j,i}}{S_{j,j}}\eta_i \right)^2 \middle| |\eta_1| > |\eta_2| > ... > |\eta_k| \right] \\ =&\mathrm{E}\left[\sum_{j=1}^{k} \sum_{i=j+1}^{k} \left(\frac{S_{j,i}}{S_{j,j}}\eta_i \right)^2 \middle| |\eta_1| > |\eta_2| > ... > |\eta_k| \right] \\ =&\sum_{j=1}^{k} \sum_{i=j+1}^{k} \left| \frac{S_{j,i}}{S_{j,j}} \right|^2 \mathrm{E}\left[\eta_i^2 \middle| |\eta_1| > |\eta_2| > ... > |\eta_k| \right] \\ =&\left| \frac{S_{1,2}}{S_{1,1}} \right|^2 \mathrm{E}[\eta_2^2] + \left(\left| \frac{S_{1,3}}{S_{1,1}} \right|^2 + \left| \frac{S_{2,3}}{S_{2,2}} \right|^2 \right) \mathrm{E}[\eta_3^2] + ... \\ &+ \left(\left| \frac{S_{1,k}}{S_{1,1}} \right|^2 + \left| \frac{S_{2,k}}{S_{2,2}} \right|^2 + ... + \left| \frac{S_{k-1,k}}{S_{k-1,k-1}} \right|^2 \right) \mathrm{E}[\eta_k^2] \end{aligned} \tag{7}$$

where $\mathrm{E}[\eta_i^2]$ is the expected value of the i^{th} entry in $\mathcal{T}$. For this particular choice of $h = \{|\eta_1| > |\eta_2| > ... > |\eta_k|\}$, the i^{th} entry in η is the i^{th} largest one, and thus $\mathrm{E}[\eta_i^2] = \mathrm{E}[\eta_{i'}^2]$. In general, $\mathrm{E}[\eta_i^2] = \mathrm{E}[\eta_{j'}^2]$ if the i^{th} entry is the j^{th} largest. The analysis for other choices of $h \in \mathcal{H}$ is analogous. Plugging (7) with the other $k! - 1$ conditional expected values into (6),

$$\mathrm{E}\left[\|\Delta\eta\|_2^2\right] \approx \frac{1}{k!}\Bigg((k-2)!\mathrm{E}[\eta_{2'}^2] + 2\,(k-2)!\mathrm{E}[\eta_{3'}^2] + \ldots + (k-1)(k-2)!\mathrm{E}[\eta_{k'}^2]\Bigg) \left(\sum_{j=1}^{k}\sum_{i\neq j}\left|\frac{S_{j,i}}{S_{j,j}}\right|^2\right). \tag{8}$$

Since the first term in (8) is independent of S,

$$\arg\min_S \mathrm{E}[\|\Delta\eta\|_2^2] = \arg\min_S \sum_{j\in\mathcal{I}}\sum_{\substack{i\in\mathcal{I}\\ i\neq j}}\left|\frac{S_{j,i}}{S_{j,j}}\right|^2. \tag{9}$$

Instead of minimizing the mutual coherence, this objective function leads to minimizing the Frobenius norm of the normalized submatrix in S corresponding to $\mathcal{I}$.

In practice, we are generally unable to identify the locations for all nonzero entries and thus $\mathcal{U} \neq \emptyset$. In this case, the whole matrix S, not only the submatrix we mentioned above, needs to be taken into account, since every column in A may correspond to $\mathcal{T}$. Based on the assumption that the nonzero entries in $\mathcal{U}$ are uniformly distributed in $\mathcal{I}^c$, (9), a slight modification of the analysis above yields,

$$\begin{aligned}\arg\min_S \mathrm{E}[\|\Delta\eta\|_2^2] = \arg\min_S &\sum_{j\in\mathcal{I}}\sum_{\substack{i\in\mathcal{I}\\ i\neq j}}\left|\frac{S_{j,i}}{S_{j,j}}\right|^2 \\ &+ \frac{k-pk}{n-pk}\left(\sum_{j\in\mathcal{I}}\sum_{i\in\mathcal{I}^c}\left|\frac{S_{j,i}}{S_{j,j}}\right|^2 + \sum_{j\in\mathcal{I}^c}\sum_{i\in\mathcal{I}}\left|\frac{S_{j,i}}{S_{j,j}}\right|^2\right) \\ &+ \frac{(k-pk)\,(k-pk-1)}{(n-pk)\,(n-pk-1)}\sum_{j\in\mathcal{I}^c}\sum_{\substack{i\in\mathcal{I}^c\\ i\neq j}}\left|\frac{S_{j,i}}{S_{j,j}}\right|^2.\end{aligned} \tag{10}$$

The optimizaiton in (10) is essentially the same as (9) with two additional weighted terms added reflecting the influence of $\mathcal{U}$. When p gets close to 1, implying we have more knowledge on the target signal, the last two terms in (10) become negligible compared to the first term and (9) becomes a close estimate for (10). For sparse signals with $k \ll n$, (9) is much more efficient than (10) in the sense of computational cost since it only considers a submatrix with k^2 entries.

The optimization problems (9) and (10) are non-convex and thus cannot be solved in polynomial time. In this paper, we use the following greedy Monte Carlo based strategy to design a μ-path sampling pattern, based on the minimization in (10).

Algorithm 1: μ-path sampling pattern design algorithm

Input: p, k, $\mathcal{I}$
Output: Sampling pattern Φ
Initialization: $\Phi = \emptyset$
while *not enough pixels sampled* **do**
  Randomly generate candidate μ-paths, μ;
  $\mu^* = \arg\min_{\Phi\cup\mu} \mathrm{E}[\|\Delta\eta\|_2^2]$;
  $\Phi \leftarrow \Phi \cup \mu^*$;
end

The algorithm starts from empty sampling set Φ. In each iteration, a certain number of μ paths are randomly generated from unsampled locations Φ^c. The one that minimizes the objective function $\mathrm{E}[\|\Delta\eta\|_2^2]$ is selected and included in Φ and the process repeated until the sampling pattern is complete.

3. SIMULATIONS

To demonstrate the effectiveness of the proposed sample path design strategy, we performed simulations on two groups of images (Fig. 2). Each group consisted of sixteen 512×512-pixel AFM images that were obtained by dividing a large material surface with the grid lines indicated in yellow. The first group (Fig. 2, left) is the surface of $BiFeO_3$/$SrRuO_3$/$DyScO_3$ and the second (Fig. 2, right) is the surface of etched silicon.

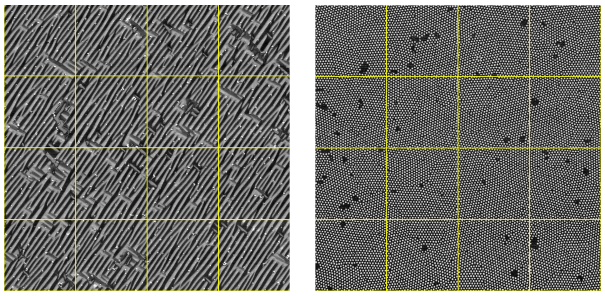

Fig. 2: Sample AFM images of two material surfaces. (Images obtained from the website of Asylum Research)

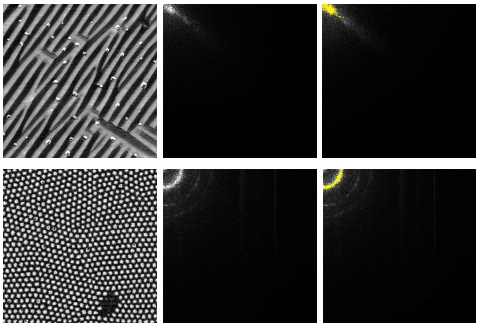

Fig. 3: (left) Sample topology AFM images, (middle) corresponding DCT domain coefficients (lighter color indicates larger coefficient) and (right) frequency structure estimations (estimated $\mathcal{I}$ is indicated in yellow).

The first image in each group (the upper-left corner image in Fig. 2) was raster scanned to estimate the frequency structure of the material. The set $\mathcal{I}$ estimated from the raster-scanned image for each material and used in the algorithm is shown in the right column of Fig. 3. Based on the frequency information, μ-path sample patterns of size 40 were generated according to Algorithm 1. In each iteration of the algorithm, 9 μ-paths were generated randomly. From these, the one minimizing $\mathrm{E}[\|\Delta\eta\|_2^2]$ was selected and included into the sampling set Φ. Iterations continuing until 20% of the total pixels were sampled. The rest of the images in each group were sampled using the designed patterns and the reconstruction was then created with the $1,200$ largest coefficients recovered by SMP. (The recovered coefficients are not necessary in the set $\mathcal{I}$.) We used (9) to approximate (10) due to the reduced computational cost. The sparsity matrix Ψ was selected to be the inverse discrete cosine transform matrix. The Peak Signal-to-Noise Ratio (PSNR) was used as the measure of image reconstruction quality.

For comparison, we also used another two μ-path pattern design strategies. The first was a random μ-path pattern as de-

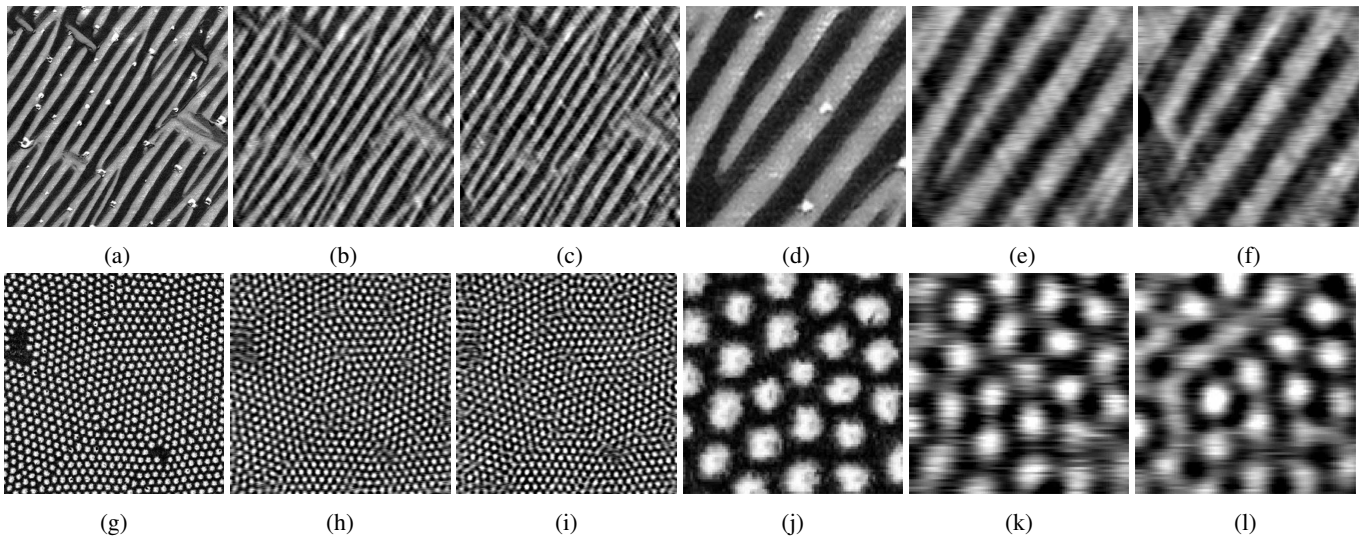

Fig. 4: Example reconstructions. (a) and (g) are original AFM images (the bottom-right corner images in Fig. 2). (b) and (h) are the reconstructions with sample patterns designed using Algorithm 1. (c) and (i) are the reconstructions with random sample patterns. The patterns used to create (b) and (c) are shown in Fig. 5. The left three columns are the details of the bottom-left corner. (d), (e), (f), (j), (k), (l) correspond to (a), (b), (c), (g), (h), (i) respectively. (Reconstruction with MCM is omitted for space reasons.)

scribed in [12]. The second was mutual coherence minimization (MCM), selected because mutual coherence minimization is a common design strategy. Designing a sampling pattern and corresponding sensing matrix A by minimizing mutual coherence is also non-convex. To find an approximate solution, we applied the same Monte Carlo-based greedy algorithm as in our approach, except that, in the second step, the objective function $\mathrm{E}[\|\Delta\eta\|_2^2]$ was replaced by the mutual coherence,

$$\mu^* = \arg\min_{\Phi\cup\mu} \left\{ \max_{\substack{i,j\in\mathcal{I}\\ i\neq j}} \left| \frac{S_{j,i}}{\sqrt{S_{j,j}S_{i,i}}} \right| \right\}. \qquad (11)$$

For each of the fifteen non-rastered images in the two groups, 10 simulations with 10 patterns created using each strategy were carried out. The average PSNR and the standard deviation for each image and strategy are presented in Table 1. Our proposed method outperformed both the random strategy and the MCM strategy in reconstruction accuracy on every image for both samples, with an average increase in PSNR of 1.47 dB over random sampling and 1.03 dB over MCM for the first image set and of 0.63 dB over random and 0.47 dB over MCM for the second set. In addition, the proposed method showed more stable reconstruction as evidenced by the smaller standard deviation in the reconstruction quality over random in every image and over MCM in 26 of the 30 reconstructions.

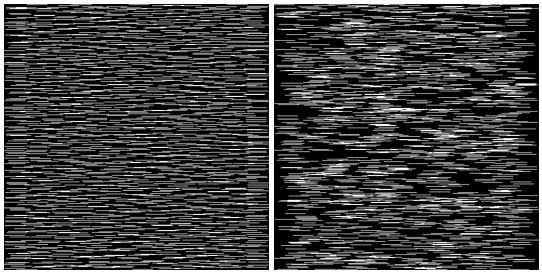

Fig. 5: μ-path sample patterns of size 40. The left image shows the sample pattern designed with Algorithm 1 and used for Fig. 4b. The right image shows the random sample pattern used for 4c. White lines indicate pixels to be sampled.

4. CONCLUSION

In this work, we have proposed a μ-path sampling pattern design strategy for effective AFM image acquisition. μ-path pattern is still a discrete sampling pattern requiring extra time to repeatedly lift and re-engage AFM tip. Future work will focus on the design of continuous patterns.

Table 1: Reconstruction quality (PSNR in dB) and standard deviation (SD) for two groups of AFM images using the proposed sampling strategy, MCM and random sampling. (image order from left to right, top to bottom)

PSNR		image 2	image 3	image 4	image 5	image 6	image 7	image 8	image 9	image 10	image 11	image 12	image 13	image 14	image 15	image 16
$BiFeO_3/SrRuO_3/DyScO_3$																
Mean	Proposed	20.0*dB*	20.5*dB*	19.8*dB*	20.2*dB*	20.3*dB*	19.9*dB*	20.0*dB*	20.4*dB*	20.3*dB*	20.4*dB*	20.6*dB*	19.7*dB*	19.8*dB*	20.6*dB*	20.4*dB*
	MCM	19.0*dB*	19.3*dB*	18.8*dB*	19.2*dB*	19.2*dB*	18.9*dB*	18.8*dB*	19.4*dB*	19.3*dB*	19.4*dB*	19.7*dB*	18.7*dB*	18.9*dB*	19.4*dB*	19.5*dB*
	Random	18.6*dB*	18.8*dB*	18.4*dB*	18.8*dB*	18.8*dB*	18.6*dB*	18.4*dB*	18.9*dB*	18.8*dB*	18.8*dB*	19.3*dB*	18.2*dB*	18.5*dB*	19.0*dB*	18.9*dB*
SD	Proposed	0.09*dB*	0.08*dB*	0.10*dB*	0.10*dB*	0.11*dB*	0.15*dB*	0.10*dB*	0.10*dB*	0.13*dB*	0.09*dB*	0.10*dB*	0.14*dB*	0.13*dB*	0.12*dB*	0.10*dB*
	MCM	0.11*dB*	0.21*dB*	0.15*dB*	0.13*dB*	0.20*dB*	0.14*dB*	0.17*dB*	0.16*dB*	0.15*dB*	0.11*dB*	0.12*dB*	0.12*dB*	0.12*dB*	0.17*dB*	0.12*dB*
	Random	0.13*dB*	0.23*dB*	0.17*dB*	0.18*dB*	0.20*dB*	0.13*dB*	0.15*dB*	0.17*dB*	0.14*dB*	0.17*dB*	0.14*dB*	0.19*dB*	0.20*dB*	0.14*dB*	0.16*dB*
Silicon																
Mean	Proposed	15.4*dB*	15.3*dB*	15.8*dB*	15.6*dB*	15.6*dB*	15.7*dB*	15.8*dB*	15.8*dB*	15.6*dB*	16.0*dB*	15.8*dB*	15.6*dB*	15.6*dB*	15.6*dB*	15.5*dB*
	MCM	15.0*dB*	14.8*dB*	15.2*dB*	15.1*dB*	15.2*dB*	15.2*dB*	15.2*dB*	15.2*dB*	15.2*dB*	15.5*dB*	15.4*dB*	15.3*dB*	15.2*dB*	15.2*dB*	15.0*dB*
	Random	14.9*dB*	14.7*dB*	15.0*dB*	14.9*dB*	15.1*dB*	15.0*dB*	15.0*dB*	15.0*dB*	15.1*dB*	15.4*dB*	15.3*dB*	15.0*dB*	15.1*dB*	15.0*dB*	14.8*dB*
SD	Proposed	0.08*dB*	0.10*dB*	0.10*dB*	0.10*dB*	0.10*dB*	0.09*dB*	0.10*dB*	0.08*dB*	0.10*dB*	0.07*dB*	0.10*dB*	0.07*dB*	0.07*dB*	0.09*dB*	0.09*dB*
	MCM	0.11*dB*	0.10*dB*	0.11*dB*	0.10*dB*	0.10*dB*	0.13*dB*	0.14*dB*	0.07*dB*	0.11*dB*	0.06*dB*	0.12*dB*	0.08*dB*	0.07*dB*	0.09*dB*	0.14*dB*
	Random	0.11*dB*	0.12*dB*	0.13*dB*	0.10*dB*	0.10*dB*	0.13*dB*	0.15*dB*	0.16*dB*	0.11*dB*	0.10*dB*	0.09*dB*	0.10*dB*	0.09*dB*	0.11*dB*	0.13*dB*

5. REFERENCES

[1] G. Schitter, K. J. Astrom, B. E. DeMartini, P. J. Thurner, K. L. Turner, and P. K. Hansma, "Design and Modeling of a High-Speed AFM-Scanner," *IEEE Transactions on Control Systems Technology*, vol. 15, no. 5, pp. 906–915, Sep. 2007.

[2] B. J. Kenton, A. J. Fleming, and K. K. Leang, "Compact ultra-fast vertical nanopositioner for improving scanning probe microscope scan speed," *Review of Scientific Instruments*, vol. 82, no. 12, p. 123703, 2011.

[3] S. Salapaka, A. Sebastian, J. P. Cleveland, and M. V. Salapaka, "High bandwidth nano-positioner: A robust control approach," *Review of Scientific Instruments*, vol. 73, no. 9, pp. 3232–3241, 2002.

[4] T. Ando, "High-speed atomic force microscopy coming of age," *Nanotechnology*, vol. 23, no. 6, p. 062001, Jan. 2012.

[5] M. Rana, H. R. Pota, and I. R. Petersen, "Model predictive control of atomic force microscope for fast image scanning," in *Proc. IEEE Conference on Decision and Control*, 2012, pp. 2477–2482.

[6] P. Huang and S. B. Andersson, "High speed atomic force microscopy enabled by a sample profile estimator," *Applied Physics Letters*, vol. 102, no. 21, pp. 213 118–213 118–4, 2013.

[7] B. Song, N. Xi, R. Yang, K. W. C. Lai, and C. Qu, "Video rate atomic force microscopy (afm) imaging using compressive sensing," in *Proc. IEEE Conference on Nanotechnology*, 2011, pp. 1056–1059.

[8] S. B. Andersson and L. Y. Pao, "Non-raster sampling in atomic force microscopy: A compressed sensing approach," in *Proc. American Control Conference*, 2012, pp. 2485–2490.

[9] Y. Luo and S. B. Andersson, "A comparison of reconstruction methods for undersampled atomic force microscopy images," *Nanotechnology*, vol. 26, no. 50, p. 505703, 2015.

[10] E. J. Candes, "The restricted isometry property and its implications for compressed sensing," *Comptes Rendus Mathematique*, vol. 346, no. 9, pp. 589–592, 2008.

[11] D. L. Donoho, M. Elad, and V. N. Temlyakov, "Stable recovery of sparse overcomplete representations in the presence of noise," *IEEE Transactions on Information Theory*, vol. 52, no. 1, pp. 6–18, 2006.

[12] B. D. Maxwell and S. B. Andersson, "A compressed sensing measurement matrix for atomic force microscopy," in *Proc. American Control Conference*, 2014, pp. 1631–1636.

[13] Y. Luo and S. B. Andersson, "A fast image reconstruction algorithm for compressed sensing-based atomic force microscopy," in *Proc. American Control Conference*, 2015, pp. 3503–3508.

[14] M. Elad, "Optimized projections for compressed sensing," *IEEE Transactions on Signal Processing*, vol. 55, no. 12, pp. 5695–5702, 2007.

[15] J. M. Duarte-Carvajalino and G. Sapiro, "Learning to sense sparse signals: Simultaneous sensing matrix and sparsifying dictionary optimization," DTIC Document, Tech. Rep., 2008.

[16] J. Xu, Y. Pi, and Z. Cao, "Optimized projection matrix for compressive sensing," *EURASIP Journal on Advances in Signal Processing*, vol. 2010, no. 1, p. 1, 2010.

[17] M. A. Davenport, A. K. Massimino, D. Needell, and T. Woolf, "Constrained adaptive sensing," *IEEE Transactions on Signal Processing*, vol. 64, no. 20, pp. 5437–5449, 2016.